CHEMISTRY OF MATERIALS

Review

pubs.acs.org/cm

Layer-by-Layer Assembly for Graphene-Based Multilayer Nanocomposites: The Field Manual

Eungjin Ahn,[†] Taemin Lee,[†] Minsu Gu,[†] Minju Park,[†] Sa Hoon Min,[†] and Byeong-Su Kim*[,†,‡]

[†]Department of Energy Engineering and [‡]Department of Chemistry, Low Dimensional Carbon Materials Center, Ulsan National Institute of Science and Technology (UNIST), Ulsan 44919, Korea

Supporting Information

ABSTRACT: With its superior electrical, optical, thermal, and mechanical properties, graphene offers a versatile platform for fabricating innovative hybrid composite materials with diverse potential applications. The preparation of graphene-based composites, particularly as thin films with nanoscale precision, is highly important for fabricating electrodes for energy and electronic devices as well as for facilitating understanding of the interplay between each component within the composites. In this context, the layer-by-layer (LbL) assembly technique offers a simple and versatile process for the fabrication of highly ordered multilayer film structures from various types of materials in a controllable manner. This paper presents details of the preparation and functionalization of these materials and the techniques for the LbL assembly of different graphene-based nanocomposites using polymers and nanoparticles. We anticipate that the protocols presented in this paper will guide researchers in the reproducible assembly of various high-quality graphene-based nanocomposites for fundamental researches and for diverse potential applications.

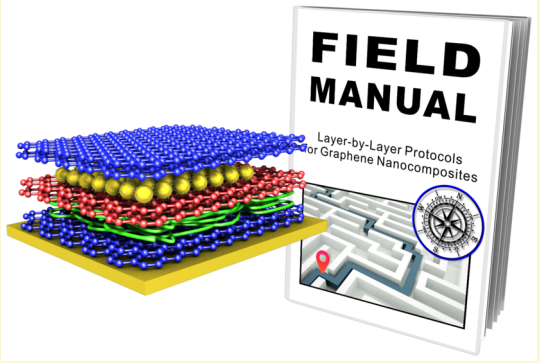

1. INTRODUCTION

Graphene, a two-dimensional single-layered carbon network, is an interesting platform material for the preparation of nanocomposites owing to its unique properties such as its large surface area (2600 m^2 g^{-1}), high conductivity (electron mobility: 15 000 cm^2 V^{-1} s^{-1}), and excellent mechanical stability (Young's modulus: 1100 GPa).[1−3] These remarkable intrinsic properties have attracted widespread interest from diverse research fields.[4−6] However, the preparation of pristine graphene is only possible through a limited number of methods, such as mechanical exfoliation[7] and chemical vapor deposition,[8,9] and both result in poor yields. The discovery of graphene oxide (GO), a product of chemical oxidation and exfoliation of graphite,[10−13] has opened an indirect pathway for utilizing the properties of graphene, albeit with some modified properties. Thus, a feasible route to harnessing the unique properties of graphene for practical applications is the incorporation of graphene derivatives into composites. In this regard, numerous graphene-based composite materials have been applied in energy storage and conversion devices such as batteries,[6,14,15] supercapacitors,[16] and solar cells,[17] and also extended toward biomedical fields as biosensors,[18] bioimaging agents,[19] and drug delivery systems.[20,21]

A critical issue in the design of graphene-based nanocomposites is the selection of suitable conjugate materials that impart synergetic effects to their composites while maintaining homogeneity within heterogeneous constituent assemblies. Toward that purpose, a technique to form uniform nanoscale composites while preserving the unique characteristics of each component is highly desirable. One method that satisfies these requirements is the layer-by-layer (LbL) assembly technique.[22−29] LbL assembly is a versatile thin-film fabrication method in which the assembly of a composite structure proceeds through the sequential adsorbing of different macromolecular materials by exploiting the intermolecular attractive forces between the components, such as electrostatic interactions,[30,31] hydrogen bonding,[32,33] and van der Waals forces.[34] Integration of graphene-based materials into LbL assembly not only introduces a new addition to the existing library of LbL materials but also brings opportunities to overcome some conventional limitations in physical and chemical properties of polymeric materials. One of the most interesting features of LbL-based graphene composites arises from the synergetic effects between graphene and its diverse conjugate materials, thus virtually unlimited multitude of composites remains to be explored. Many of recent advances in graphene-based LbL assembly are extensively listed in the table of our previous contribution.[35]

Since the inspirational study on LbL-assisted graphite oxide nanocomposites conducted by Kotov et al.,[36] many researchers, including ourselves, have devoted significant effort to the field

Special Issue: Methods and Protocols in Materials Chemistry

Received: July 1, 2016
Revised: October 9, 2016
Published: October 10, 2016

DOI: 10.1021/acs.chemmater.6b02688
Chem. Mater. 2017, 29, 69−79

of graphene-based nanocomposite thin films containing components such as carbon nanomaterials, polymers, and metal nanoparticles (NPs).[37−47] As representative examples, the Tsukruk group has pioneered the mechanical analysis of LbL-assembled graphene multilayer composites;[40] Ariga and co-workers have successfully demonstrated the use of graphene-based thin-film composites for highly sensitive sensors.[41] The Kotov group has also provided clear structural insight into LbL-assembled GO and polymer composites;[44] Furthermore, our group has demonstrated the utility of LbL-assembled GO-based multilayers for electronic,[42] catalytic,[43] mechanical,[46] and biological applications.[45] The aforementioned studies mainly used graphene as a platform to enhance the characteristics of the conjugate materials, such as their conductivity, mechanical properties, and catalytic activity. For further information on these studies and for more examples of graphene-based nanocomposites, see the several excellent reviews in the literature.[4,28,29,35,48,49]

Despite the considerable progress made in this field, a well-established protocol for the assembly of graphene-based LbL nanocomposites remains to be formulated. Consequently, on the basis of the experience and knowledge that our group has developed over the past six years, we present herein a detailed protocol for fabricating LbL assemblies, including preparation methods for the necessary substrates and suspensions, and discuss the possible future applications of such assemblies. The main objective of this paper is to share reliable procedures with researchers in the field and also to guide new researchers to broaden the horizon of graphene-based nanocomposite materials.

2. PROCEDURES AND RESULTS

LbL assembly is a rational strategy used to construct multilayered nanocomposites based on the attractive forces between macromolecular components. For graphene-based multilayer nanocomposites, we focused on LbL assemblies that exploit electrostatic interactions and proceeded by the sequential deposition of positively and negatively charged components (Scheme 1). The incorporation of positive and negative charges into the components and the stabilization of their aqueous suspensions are therefore essential for LbL assembly.

The synthetic procedures in this manual were organized to address the preparation of three representative graphene-based multilayer nanocomposites with a workflow comprising five main steps: (i) preparation and (ii) characterization of the suspension, (iii) substrate treatment, (iv) LbL assembly, and (v) film characterization (Scheme 1). To provide an insight into the combination of materials in multilayered nanocomposites, three LbL assemblies were conducted, one using a two-dimensional (2D) graphene derivative, one using a one-dimensional (1D) polymer, and one using a zero-dimensional (0D) metal NP, all of which were composited with 2D GO nanosheets as a basic building block.

2.1. Suspension Preparation. *GO(−).* Chemically derived GO nanosheets are a fundamental material in graphene-based multilayer nanocomposites. The abundant oxygen functional groups allow GO nanosheets to maintain a stable dispersion in aqueous suspension despite their large lateral dimension (ca. 1 μm). Thus, the aqueous GO suspension, denoted as GO(−), itself can act as a negatively charged component in LbL assemblies without additional functionalization. Although there are a number of methods for the preparation of GO outlined recently, we introduce our synthetic protocol to guarantee the reliable preparation of GO suspension we used. Hummers' method, a strong oxidation and exfoliation process, is the most commonly employed approach to prepare GO nanosheets for bulk-scale synthesis. Here, GO nanosheets were prepared by a modified two-step Hummers' oxidation process without using $NaNO_3$, thus avoiding the generation of toxic gases.[50]

Scheme 1. General Workflow and Illustration of LbL Assembly

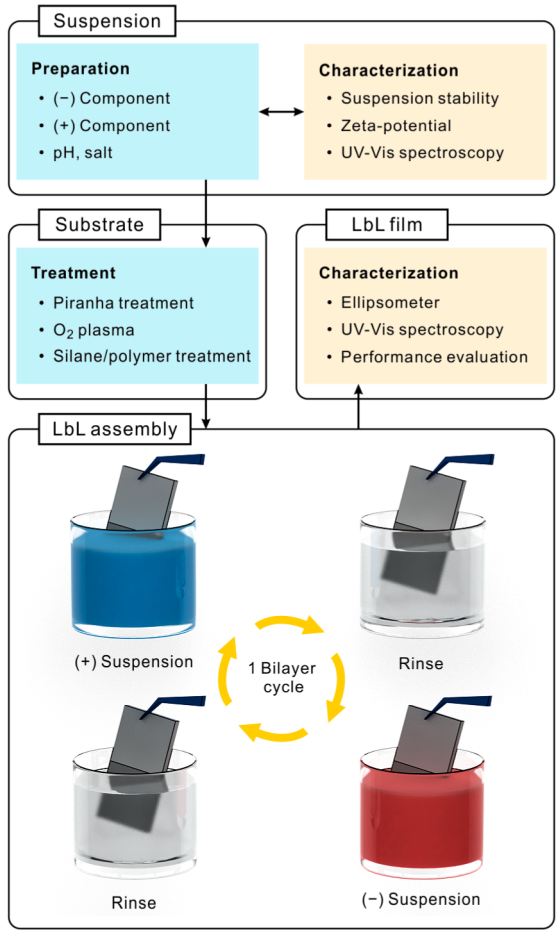

Pretreatment and Oxidation of Graphite (Timing: 2 days)

1. Graphite powder (1.0 g), potassium persulfate, ($K_2S_2O_8$, 0.50 g), and phosphorus pentoxide (P_2O_5, 0.50 g) are added to 3.0 mL of concentrated H_2SO_4 in a 50 mL round-bottom flask with stirring until the reactants are completely dissolved.
2. The mixture is kept at 80 °C for 4.5 h using a hot plate, after which the reaction is stopped and the mixture is diluted with 1.0 L of deionized (DI) water.
   ! CAUTION: Add the graphite slurry carefully to the DI water. This mixing process induces a rapid increase in the temperature of the mixture.
3. The mixture is filtered through a glass fiber filter membrane (pore size: 1.5 μm) and is thoroughly washed with DI water to remove all traces of acid.
4. The solid is transferred to a drying dish and left overnight under ambient conditions.
5. The pretreated graphite, which is black in color, is added to 26 mL of H_2SO_4 in a 250 mL round-bottom flask, and

DOI: 10.1021/acs.chemmater.6b02688
Chem. Mater. 2017, 29, 69−79

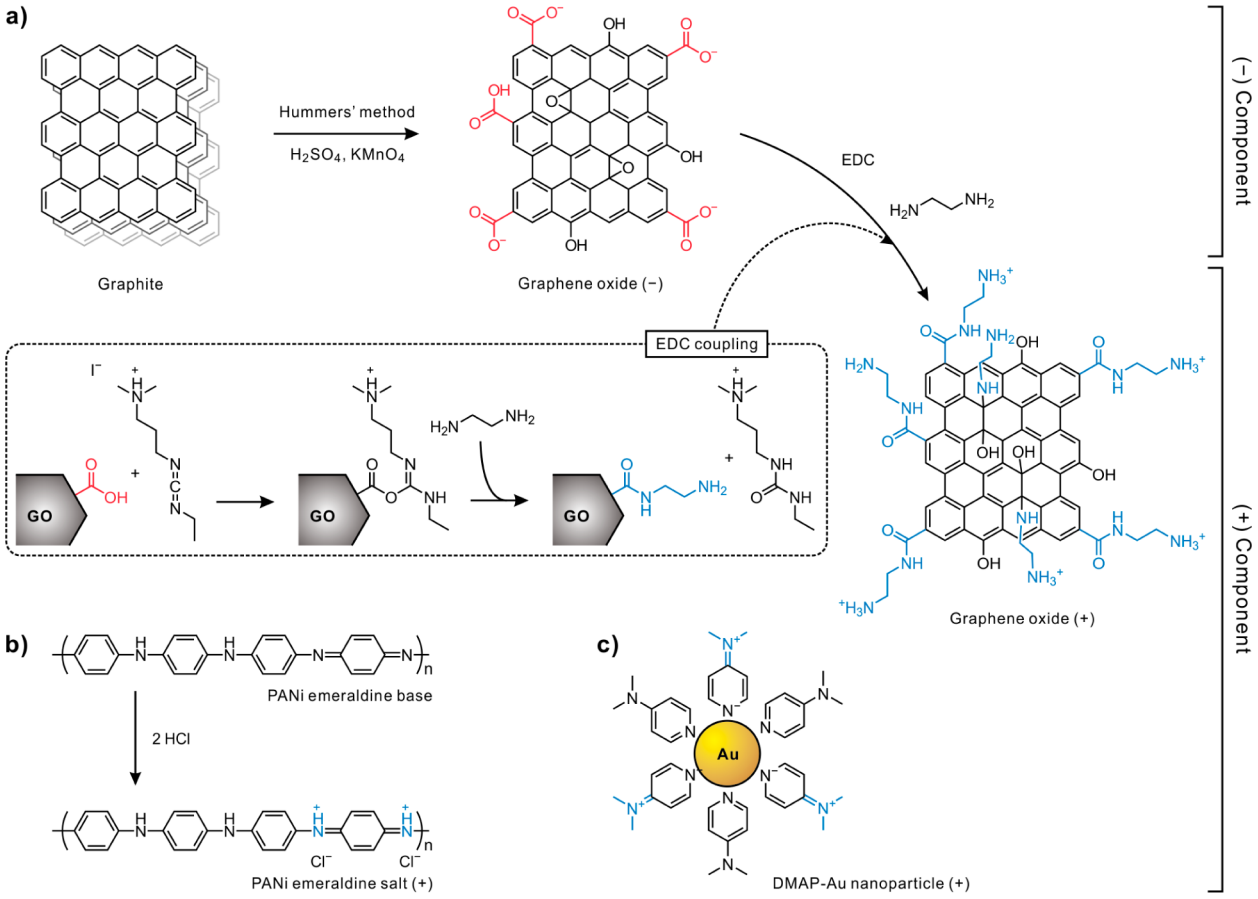

Figure 1. (a) Synthetic procedure for GO and amine-functionalized GO. Molecular structures of positively charged (b) polyaniline (PANi) and (c) 4-(dimethylamino)pyridine (DMAP)-Au NP.

the mixture is stirred until a homogeneous dispersion is achieved.

6. The flask is placed in an ice bath and potassium permanganate ($KMnO_4$, 3.0 g) is added slowly, ensuring that the temperature remains below 10 °C.

   ! CAUTION: The addition of $KMnO_4$ causes a rapid increase in temperature. Thus, the rate of addition must be carefully controlled to prevent the suspension temperature from exceeding 10 °C.

7. The reaction is warmed to 35 °C and reacted for 2 h. After then, the flask is placed in an ice bath and DI water (46 mL) is carefully added into the mixture.

   ! CAUTION: Because the addition of water to H_2SO_4 also causes a rapid increase in the solution temperature, it should be carried out in an ice bath so that the temperature does not exceed 10 °C.

8. This mixture, which is dark-brown in color, is further stirred for 0.5 h at 35 °C, after which heating is stopped and the mixture is diluted with 140 mL of DI water. Then, 30% hydrogen peroxide (2.5 mL) is added to the mixture, resulting in a bright yellow intermediate solution that effervesces.
9. The suspension is allowed to settle for at least 1 day.

Purification of GO (Timing: 2 weeks)

10. The clear supernatant solution is removed, and the remaining precipitate is thoroughly washed with a 10% HCl solution (1.0 L) to remove any metallic impurities. Then, the washed solution is removed by filtration through a glass fiber filter membrane, affording a soil-like product, which is dark-yellow in color.

    KEY POINT: Unlike the first filtration process in the pretreatment step, the second filtration might take longer. Do not filter the entire precipitate at once.

11. The resulting solid is dried in air and redispersed in DI water. The dispersion is then placed in a dialysis membrane and dialyzed exhaustively against DI water for 2 weeks to remove any remaining metal or chemical residues.
12. The product is centrifuged and washed several times with DI water in order to neutralize it and remove any residual species.
13. Finally, the dark brown GO powder is dried at 50 °C in a vacuum oven for 1 day.
14. A sample of GO powder (50 mg) in DI water (100 mL) is subjected to ultrasonication at 35 W for 40 min to obtain a stable suspension. The suspension is then centrifuged at 4000 rpm for 10 min, and the top 90% of the supernatant is used for LbL assembly. The thickness and lateral dimension of exfoliated GO(−) sheets were characterized by AFM and SEM (see Figure S1 in the Supporting Information).

GO(+). To construct all graphene-based multilayer nanocomposites, we prepared a positively charged form of GO, denoted as GO(+), by amine functionalization of GO nanosheets. 1-[3-(Dimethylamino)propyl]-3-ethylcarbodiimide methiodide (EDC) is an efficient coupling agent for the formation of amide bonds in the aqueous phase. The carboxylic

DOI: 10.1021/acs.chemmater.6b02688
Chem. Mater. 2017, 29, 69−79

acids in GO can be replaced with amine groups by the formation of amides using ethylenediamine. This reaction proceeds via an unstable ester intermediate that is formed between the carboxylic acid groups and EDC (Figure 1a).[21,51,52]

Amine Functionalization of GO (Timing: 3−4 days)

1. GO powder (50 mg) is dispersed in DI water (100 mL) with ultrasonication for 40 min at a concentration of 0.50 mg mL^{-1}.
2. EDC (1.25 g) is added to the GO solution (100 mL) with vigorous stirring. Ethylenediamine (10 mL) is added immediately and the solution is stirred overnight at room temperature.

   KEY POINT: EDC is moisture-sensitive and should be stored in a refrigerator at ca. −10 °C. Before opening the chemical container, be sure to keep it at room temperature for 30 min to avoid condensation and deactivation of the EDC.

   ! CAUTION: Ethylenediamine is a highly corrosive and flammable liquid. Avoid breathing its vapor and wear a lab coat, gloves, and goggles during the experiments.
3. The synthesized suspension is then dialyzed exhaustively for ca. 3 days in 1.0 L of DI water to remove the remaining reagents and byproducts. The DI water is changed frequently at the beginning of dialysis, and the pH of the dialysate is regularly checked. The dialysis is finished when the pH of the dialysis fluid is neutral.

PANi(+). PANi was employed as a representative polymeric component for LbL assembly. Because the emeraldine salt form of PANi possesses positively charged functional groups under acidic pH (Figure 1b), PANi can be used as a counterpart for the GO(−) component in LbL assemblies. An aqueous suspension of PANi, denoted as PANi(+), was prepared by dissolving the emeraldine base form of PANi in dimethylacetamide (DMAc) and then diluting with pH-adjusted water according to a method previously reported in the literature (see Supporting Information).[53]

Au NP(+). As an example of LbL assembly between metal NP and GO nanosheets, we employed ligand-stabilized Au NP as a counterpart for GO(−). Monodispersed Au NP was synthesized in an organic solvent, and then transferred into an aqueous solution containing DMAP ligands. DMAP stabilization imparts positive charge to the surface of Au NPs and allows the stable dispersion of Au NPs as an aqueous suspension (Figure 1c).[54] The prepared Au NP suspension is denoted as Au(+) (see Supporting Information).

2.2. Suspension Characterization. *Colloidal Stability.* The surface charge density of LbL components plays a fundamental role in the alternating assembly of oppositely charged components. The suspension stability is another key factor in the preparation of uniform assemblies of multilayered nanocomposites.[55] The surface charge density and suspension stability can be highly dependent on the pH of the suspension by the protonation/deprotonation state of the functional groups in the LbL components. Thus, the suspension pH should be adjusted prior to LbL assembly. We measured the ζ-potential of each suspension in the pH range of 3 to 11, as shown in Figure 2b. In the wide range of pH condition, strong negative and positive charges were observed in GO(−) and GO(+), with the average ζ-potentials of −48.2 ± 10.1 mV and +48.8 ± 6.1 mV, respectively. The chemically derived GO suspensions also exhibited high dispersion stability, owing to

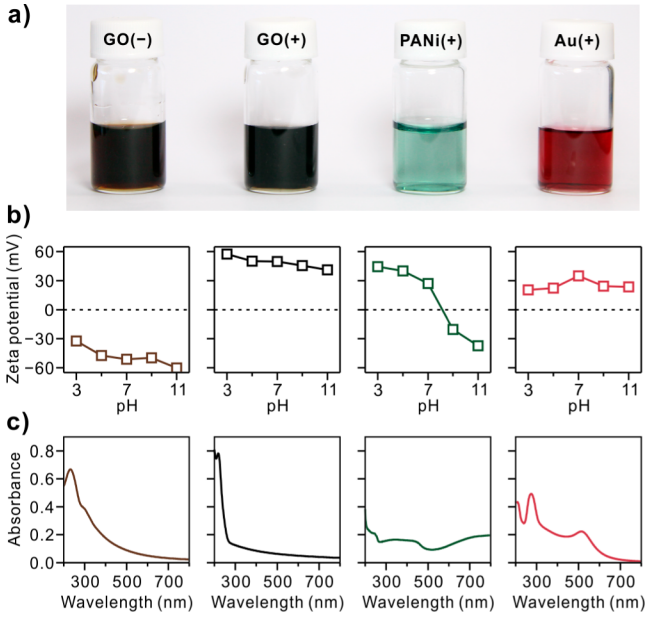

Figure 2. (a) Photographs, (b) ζ-potentials under different pH conditions, and (c) UV−vis spectra of GO(−), GO(+), PANi(+), and Au(+) suspensions (from left to right).

the presence of the functional groups on the surface of the GO nanosheets. PANi(+) exhibited positive charge under acidic conditions and formed a stable dispersion in aqueous suspensions, but irreversible aggregation was observed under alkaline conditions, resulting from the deprotonation of the PANi backbone.[56] In contrast, the color of Au(+) changed from red to violet below pH 7, indicating the aggregation of unstable Au NPs. Therefore, the pH values of the PANi(+) and Au(+) suspensions were fixed at 2.5 and 11, respectively, for LbL assembly.

Absorbance Spectra. The UV−vis absorbance spectra of GO(−) exhibited two characteristic peaks at 235 and 300 nm, corresponding to $\pi-\pi^*$ transitions of aromatic C═C bond in the sp^2 region and $n-\pi^*$ transitions of C═O bonds, respectively.[54] The two characteristic peaks were blue-shifted to 200 and 219 nm in GO(+) by amine functionalization.[49] The absorbance peaks of PANi(+) at 310−330 nm and 380−410 nm corresponded to $\pi-\pi^*$ transition and the polaron band, respectively.[57] In addition, the absorbance at 274 and 513 nm of Au(+) represents the characteristic peak of DMAP and the surface plasmon absorbance of Au NPs, respectively. These characteristic peaks suggest the formation of stable aqueous suspensions of the Au(+) for LbL components.[54]

2.3. LbL Assembly of Graphene Nanocomposites. *Substrate Treatment.* Because the first component directly contacts the substrate, substrate treatments that induce the formation of charged functional groups are crucial to enhance electrostatic interactions between the substrate and the first LbL component. In most cases, negatively charged substrates are used to assemble a positively charged component as the first deposition layer. However, negatively charged GO nanosheets should be the first deposition layer for the efficient loading of positively charged Au NPs. Thus, positively charged substrates are also necessary in some cases. The type of substrate should be chosen depending on the application. To remove any organic contamination, an indium tin oxide (ITO)-coated glass substrate was cleaned by sonication in DI water, acetone, and

DOI: 10.1021/acs.chemmater.6b02688
Chem. Mater. 2017, 29, 69−79

ethanol for 10 min each. Silicon and quartz substrates were cleaned in piranha solution (H_2SO_4:H_2O_2 7:3 v/v) for 1 h. The negatively and positively charged surfaces were obtained by oxygen (O_2) plasma treatment for 10 min and by dipping in (3-aminopropy)triethoxysilane (APTES) solution (10% v/v in ethanol) for 4 h, respectively.[38]

! CAUTION: Piranha solution is dangerous and extremely reactive with organic substances. Appropriate safety precautions should be taken.

KEY POINT: After the APTES treatment, the substrate was thoroughly washed with ethanol to remove weakly bound excess residual molecules from the surface.

USEFUL TIP: A Si wafer (SiO_2 thickness near 300 nm) is an excellent substrate to confirm the successful formation of multilayers because it exhibits color variations with thin film thickness changes at the nanometer scale that are visible with the naked eye.

LbL Assembly. We applied a spin-assisted dipping (spin-dipping) method using automation equipment from nanoStrata Inc. (Figure 3). The spin-dipping method with rinsing steps

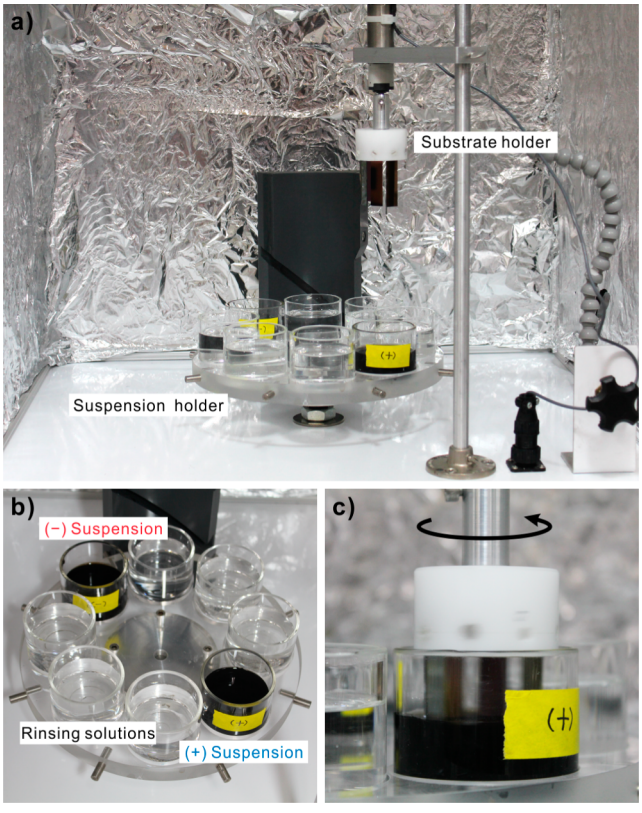

Figure 3. (a) Automated LbL assembly setup for graphene-based LbL assembly (nanoStrata). (b) Suspensions for (+) and (−) components with rinsing solutions with $(GO/GO)_n$ multilayers are used as a representative example. (c) Spin-dipping assembly (see Video S1 and Figure S2 for actual operation process).

enables the LbL components to assemble onto the substrate with a uniform layered structure.[53,58] During LbL assembly, the film structure is influenced by the suspension conditions, such as pH, ionic strength, and concentration. Of these, the pH of the suspension is the most important factor because it affects the charge density of the functional groups in the components. Like other weak polyelectrolytes commonly employed in LbL assembly, GO(−) and GO(+) are also highly sensitive to the pH of the suspension, owing to their carboxylic acid and amine groups, respectively. Moreover, the charge density determines the amount of deposition through the charge balance between the oppositely charged components, leading to different thickness, roughness, and internal structures for the resulting films.[59] Thus, the suspension pH should be chosen according to the pK_a value of the functional groups in the components and should be optimized using proper film characterization.

$(GO/GO)_n$ Films (Timing: 30 min per bilayer (BL))

USEFUL TIP: The suitability of the suspensions can be estimated before performing LbL assembly by simply mixing two oppositely charged suspensions in a small vial. If the suspensions are suitable, you could observe an instant aggregation owing to the attraction between the components.

1. The negatively charged substrate is dipped and spun for 10 min in 50 mL of GO(+) solution (0.50 mg mL^{-1}, pH 3.0) for the first step of LbL assembly. In this process, the electrostatic interaction between the negatively charged substrate and the GO(+) solution induces the formation of a fine monolayer on the substrate with a commensurate reversal of surface charge.

   USEFUL TIP: Considering the meniscus level of suspensions and to guarantee a qualified assembly onto the targeted area, the amount of suspension is determined to cover 25% extra area larger than the targeted area of the substrate (e.g., 2.5 cm dipping depth is required for assembling 2.0 cm film).
2. The GO(+)-adsorbed substrate is then rinsed three times (1 min for each step) with 60 mL of DI water (pH 3.0) to remove the loosely adsorbed excess GO off from the substrate.

   KEY POINT: Generally, more rinsing solution is employed than that used for the suspensions in order to ensure the thorough washing of polyelectrolytes from the substrate.
3. Next, the substrate is dipped and spun for 10 min in 50 mL of GO(−) solution (0.50 mg mL^{-1}, pH 3.0), following the same process as step 1, and the rinsing step is performed with pH-adjusted DI water.

   KEY POINT: To achieve high mass loading of the GO sheet in LbL assembly, GO(−) suspension (pH 3.0) is adopted in which the absolute ζ-potential value is low compared to that under other pH conditions.
4. These LbL steps assemble one BL of a GO(+)/GO(−) film, and the procedure is repeated to achieve the desired number of BLs. The substrate is dried under a gentle nitrogen stream only after the desired number of bilayers is deposited. The multilayer is typically denoted by $(GO/GO)_n$, where n indicates the number of bilayers deposited. As a convention, the first layer component indicated is a positively charged species and the latter is a negatively charged species.

   USEFUL TIP: If an additional reduction is needed, as-assembled $(GO/GO)_n$ films are placed in a tube furnace to perform thermal reduction at various temperatures (typically above 700 °C) for 1 h under Ar atmosphere.

$(PANi/GO)_n$ Films (Timing: 30 min per BL)

1. Negatively charged substrates are dipped and spun for 10 min in 50 mL of PANi(+) solution (2.0 mg mL^{-1}, pH 2.5) for the first step of LbL assembly.
2. PANi(+)-adsorbed substrates are then rinsed three times (1 min for each step) with 60 mL of DI water (pH 2.5)

DOI: 10.1021/acs.chemmater.6b02688
Chem. Mater. 2017, 29, 69−79

to remove the loosely adsorbed excess PANi from the substrate.

3. Next, the substrates are dipped and spun for 10 min in 50 mL of GO(−) solution (0.50 mg mL^{-1}, pH 3.0), following the same process as that in step 1, and the rinsing step is performed with pH-adjusted DI water.
4. These LbL steps assemble one BL of a PANi(+)/GO(−) film, and the procedure is repeated to achieve the desired number of BL in a format of $(PANI/GO)_n$. The substrate is dried under a gentle nitrogen stream only after the desired number of bilayers is deposited.

$(Au/GO)_n$ Films (Timing 30 min per BL)

1. Positively charged substrates are dipped and spun for 10 min in 50 mL of GO(−) solution (0.50 mg mL^{-1}, pH 4.0) for the first step of LbL assembly.
2. GO(−)-adsorbed substrates are then rinsed three times (1 min for each step) with 60 mL of neutral DI water to remove the loosely adsorbed excess GO(−) from the substrate.
3. Next, the substrates are dipped and spun for 10 min in 50 mL of an Au(+) suspension (pH 11), following the same process as that in step 1, and the rinsing step is performed with the neutral DI water.

   KEY POINT: To achieve high mass loading of Au NPs in LbL assembly, a stable Au(+) suspension at pH 11 is adopted in which the absolute ζ-potential value is relatively low compared with those under other basic pH conditions.
4. These LbL steps assemble one BL of Au(+)/GO(−) film, and the procedure is repeated to achieve the desired number of BL in a format of $(Au/GO)_n$. The substrate is dried under a gentle nitrogen stream only after the desired number of bilayers is deposited.

   USEFUL TIP: To investigate the electrochemical properties of these films, as-assembled $(Au/GO)_n$ films are placed in an oven to perform thermal reduction at 150 °C for 12 h in order to promote enhanced film integrity prior to the analysis.

pH Effect in LbL Assembly. The assembly pH is one of the most critical factors in determining the thickness and composition of the LbL assembly. Using LbL assembly of $(GO/GO)_n$ multilayers as a representative example, we prepare three assembly conditions such as pH 3/3, 3/7, and 3/11 for GO(+)/GO(−), respectively. An interesting difference between weak polyelectrolyte such as poly(acrylic acid) (PAA) and GO(−) lies in the degree of ionization at low pH; for example, the degree of ionization of PAA approaches zero, while GO(−) still bears enough negative charge to maintain stable dispersion at pH 3 (ζ-potential of −32.3 mV) due to the stabilization of carboxylic acid groups adjacent to aromatic sp^2-carbon backbone. In accord with this observation, the nominal pK_a values of negatively charged GO(−) were determined in the range of 4 and 10, which corresponded to ionization of different functionalities present on GO, including carboxylic acids conjugated to sp^2-carbon backbone ($pK_{a1} \sim 4$), free carboxylic acids ($pK_{a2} \sim 6$), and phenol groups ($pK_{a3} \sim 10$).[60] As such, we tailored the pH of GO(−) suspension at pH 3 (3% ionized), 7 (64% ionized), and 11 (97% ionized), respectively, while fixing the pH of GO(+) at 3 in order to maintain the sufficient positive charges (see Supporting Information).

Figure 4 shows the successful linear growth of $(GO/GO)_n$ multilayer at various pH conditions as a function of the number

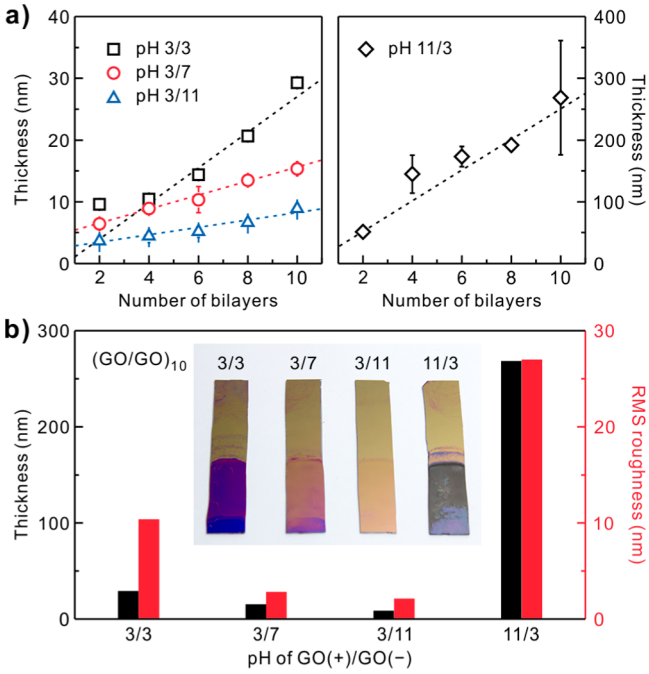

Figure 4. (a) Thickness profiles of $(GO/GO)_n$ film assembled at pH 3/3 (squares), 3/7 (circles), 3/11 (triangles), and 11/3 (diamonds). The number/number notation indicates the respective pH condition of assembled GO(+)/GO(−) suspensions. (b) Thickness and RMS roughness of $(GO/GO)_{10}$ films assembled in the different pH conditions. Inset image shows each $(GO/GO)_{10}$ film deposited on a Si wafer. Thickness and RMS roughness was measured by ellipsometry and AFM, respectively.

of bilayers. Notably, there was a difference in the characteristic reflective color of thin films assembled on silicon wafer due to the thickness difference, which could be further determined by ellipsometry yielding an average bilayer thickness of 3.06 nm (pH 3/3), 2.08 nm (pH 3/7), and 1.07 nm (pH 3/11) with respect to the assembly pH. It is shown that the average bilayer thickness of $(GO/GO)_n$ multilayer increased as the pH of the GO(−) suspension is increased, clearly reflecting the varying charge densities of the GO(−) nanosheets. The low pH condition will induce lower charge density of GO(−) owing to the protonation of carboxyl functional groups, which in turn requires more amount of GO(−) nanosheets adsorbed onto the preadsorbed GO(+) nanosheets during the LbL assembly. This charge compensation at pH 3 leads to thickest film among all assembly pH conditions tested. For comparison, we also performed the assembly of $(GO/GO)_n$ multilayer films at pH 11/3 of which each GO suspension presents the least charge density. Specifically, amine groups in GO(+) are mostly deprotonated at pH 11, whereas carboxylic acid groups in GO(−) are considerably protonated at pH 3. As a result, we found extraordinary growth of film with a thickness of approximately 270 nm of $(GO/GO)_{10}$ multilayer and a high surface roughness at pH 11/3 condition (Figure 4b).

2.4. Film Characterization. *Thickness and UV−vis Absorbance.* The growth of multilayered graphene nanocomposites is easily confirmed by the naked eye, as shown in Figure 5a. The layer growth can be also monitored using an ellipsometry, a surface profiler, UV−vis spectroscopy, or a quartz crystal microbalance for quantitative analysis. These analyses make it possible to optimize the LbL process and can help correlate device performance with the number of BLs. The

DOI: 10.1021/acs.chemmater.6b02688
Chem. Mater. 2017, 29, 69−79

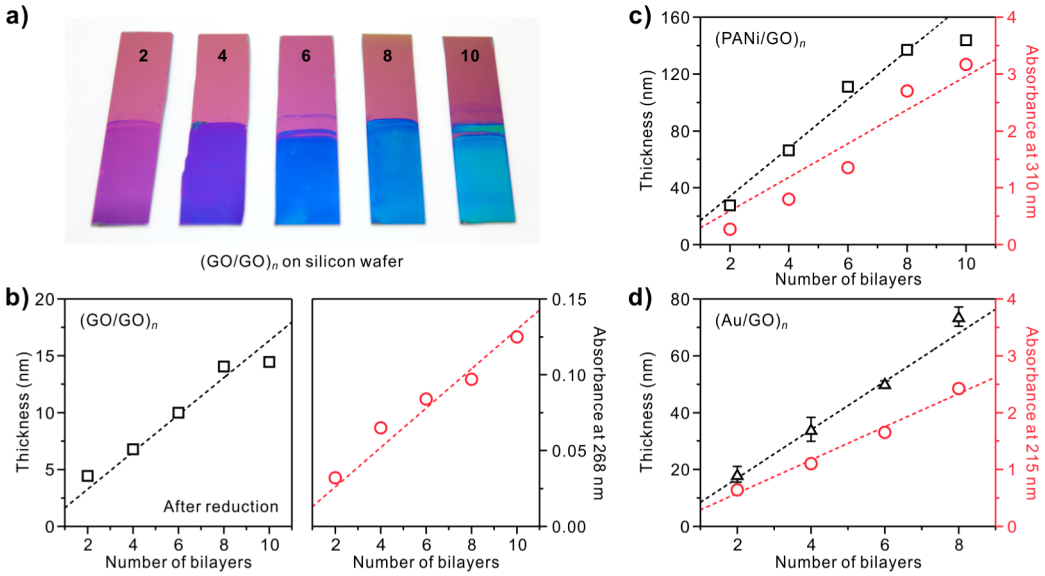

Figure 5. (a) Photograph of $(GO/GO)_n$ films deposited on a Si wafer. *n* represents the number of bilayers. Thickness profiles by ellipsometry (squares) and surface profiler (triangles), and absorbance plots (circles) of as-assembled (b) $(GO/GO)_n$ after thermal reduction, (c) $(PANi/GO)_n$, and (d) $(Au/GO)_n$ films as a function of the number of bilayers. Characteristic absorbance peaks corresponding to the active components within the multilayer are used to probe the growth of the multilayers; for example, reduced GO (268 nm), PANi (310 nm), and GO (215 nm).

average BL thickness in the $(GO/GO)_n$, $(PANi/GO)_n$, and $(Au/GO)_n$, films is 1.37, 17.73, and 8.61 nm, respectively (Figure 5b–d). In addition, the linear increase in the UV–vis absorbance corresponds to that in the film thickness. This result indicates that graphene-based LbL assembly provides a uniform and precise stacking of GO and its counterpart with commensurate linear film growth, in contrast with the nonlinear growth exhibited by some other LbL films.[61,62]

Surface Morphology. Scanning electron microscopy (SEM) and atomic force microscopy (AFM) images show the surface morphologies of the LbL components and confirm that the substrates are covered with a smooth surface with the characteristic wrinkled surfaces of GO nanosheet (Figure 6). The surface roughness values (R_q) of $(GO/GO)_6$, $(PANi/GO)_6$, and $(Au/GO)_6$ were 4.75, 16.6, and 7.07 nm, respectively. These results indicate that the morphology and roughness of the LbL films are well correlated with the dimensions of the LbL components.

2.5. Potential Applications. We have presented detailed protocols for constructing three different nanocomposite structures (GO/GO, PANi/GO, and Au/GO), including details of the suspension and substrate preparations, the LbL assembly processes, and all necessary and commonly adopted characterizations. Taking advantages of the versatility of LbL assembly, we can create multifunctional composite platforms by selecting the diverse counterpart materials and controlling the LbL engineering. This methodology is highly applicable to a wide range of research fields such as electronics, energy, catalysis, and biomedicine.

As shown in Figure 7, we explored the various applications of LbL-assembled graphene nanocomposites based on different combinations of graphene and functional materials and evaluated their performance as a function of the film thickness (i.e., number of BL). The $(GO/GO)_n$ films following thermal reduction (1000 °C for 1 h under Ar) were demonstrated as transparent conducting films that showed gradual changes in their electrical conductivity and transparency as a function of

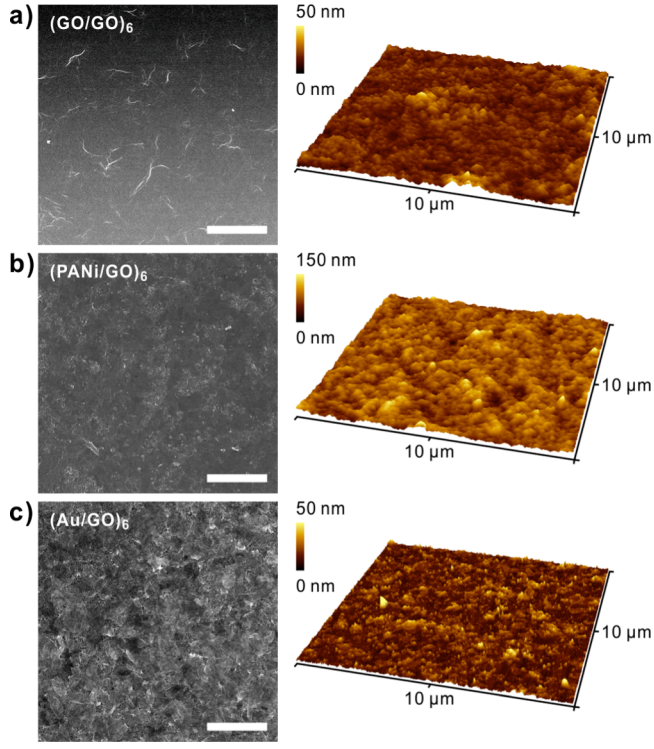

Figure 6. SEM (left) and AFM (right) surface morphology of as-assembled (a) $(GO/GO)_6$, (b) $(PANi/GO)_6$, and (c) $(Au/GO)_6$ films. All scale bars in SEM images are 2 μm.

the number of bilayers (10 kΩ sq^{-1} with 87% transmittance at 10 BL).[42]

A supercapacitor electrode was fabricated from the assembled $(PANi/GO)_n$ films. Interestingly, its overall capacitance increased with the number of bilayers (322.7 F g^{-1} at 30 BL); however, the specific capacitance per bilayer gradually decreased beyond 10 BL (24.6 F g^{-1} per BL). This indicates that achieving a fine balance between the electron

DOI: 10.1021/acs.chemmater.6b02688
Chem. Mater. 2017, 29, 69–79

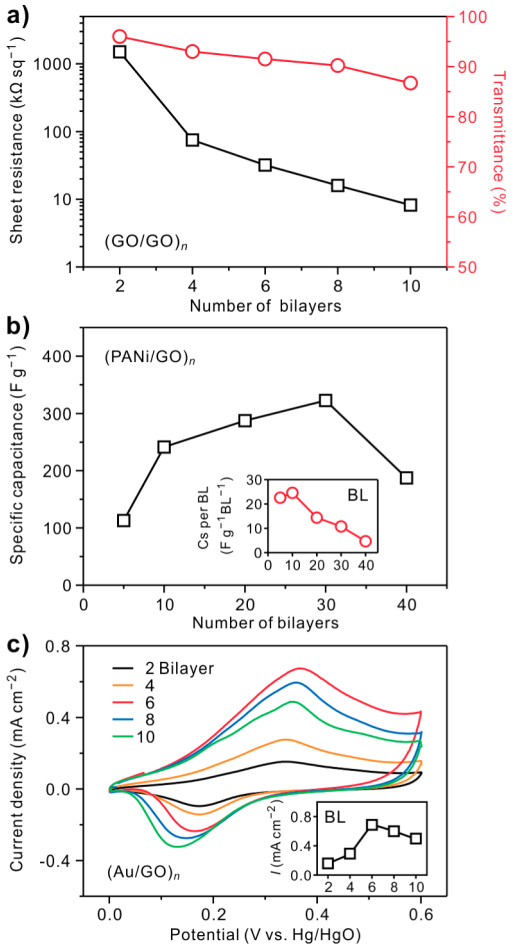

Figure 7. Application of LbL-assembled (a) $(GO/GO)_n$ films as transparent conducting films. Reproduced with permission from ref 42. Copyright 2011 The Royal Society of Chemistry. (b) $(PANi/GO)_n$ films as supercapacitors. Reproduced with permission from ref 63. Copyright 2012 The Royal Society of Chemistry. (c) $(Au/GO)_n$ films as electrocatalysts. Reproduced with permission from ref 43. Copyright 2012 John Wiley and Sons. The insets of panels b and c show the specific capacitance per BL and the peak current density plot as a function of the number of BLs.

transfer from the electrode and the ionic transport from the electrolyte is critical for high capacitive behavior.[63] In another notable example, the $(Au/GO)_n$ films were employed as electrocatalysts in the methanol oxidation reaction. The optimum catalytic performance was achieved by a 6 BL film, which exhibited high catalytic activity (273 A g^{-1}) and good cycling retention (88% over 100 cycles). Due to the limited diffusion of methanol into the hybrid electrode as well as to the reduced electron transfer to outer NPs, increased thickness over 6 BL showed decreased catalytic activities.[43]

Thus, the optimum performance of each graphene nanocomposite is strongly correlated to the selection of materials and the film thickness. This finding indicates that precise control of the desired functionalities of multilayered films is necessary and possible by taking advantage of the LbL-based nanoscale engineering of the electrode.

Although we mainly utilized the LbL-assembled graphene nanocomposites for energy applications, they have enormous potential in many fields of science and engineering owing to their tailorable architectures, compositions, and tunable properties. Considering the simplicity and versatility of this methodology, we anticipate that the LbL approach will emerge as the attractive platform technique for the design and fabrication of diverse hybrid nanocomposites with tailored functionalities.

2.6. New Challenges in LbL-Assembled Graphene Nanocomposites. We anticipate that unexplored fundamental studies and design strategies for LbL assembly composites remain to be discovered, and some of their future endeavors are proposed in the following.

Structural Control of Graphene Sheet. Until now, chemically exfoliated graphene has been extensively utilized in various fields as a versatile platform due to its superior intrinsic properties together with a facile preparation method. It is well-known that the physicochemical properties of graphene sheets are highly dependent on their chemical compositions such as sheet size, density of functional groups, heteroatom doping, and defect density. The electronic and mechanical properties of the nanocomposites will be benefited from the larger sized graphene sheets with less defect density. On the other hand, smaller sized graphene sheets show high dispersion stability in various media, providing improved processability for composite applications. Thus, more controlled synthesis of graphene with well-defined structures and compositions not only expands the versatility of composite materials for diverse applications but also helps to provide the fundamental understanding of graphene-based LbL assembly.

Multicomponent Assembly and Architecture Control. Although most of LbL-assembled composites are based on the two-component assembly, multicomponent assembly beyond the conventional approach will be a subject of intensive research effort in LbL systems. Moreover, the internal architecture of composites is easily tunable by simply adjusting the layer sequence, resulting in various nanocomposites with controlled structures. For example, with a simple two-component system composed of active species of A and B, one could produce the fully alternating structure (i.e., substrate/ABAB) or compartmented structure (i.e., substrate/AABB or substrate/BBAA). This precise control of internal structure within the thin films can optimize the characteristics of the LbL-assembled graphene nanocomposites even under the identical composition, which is not attainable with a simple mixing method.

Novel Building Blocks. Diverse materials are widely used for LbL components, regardless of the chemical compositions (e.g., organic, inorganic, carbon, and metal) and their dimensions (e.g., 0-, 1-, 2-, and 3D). Recent developments in materials science have continuously expanded the potential candidates for LbL components, including metal dichalcogenides such as MoS_2 and WS_2. Based on the discovery of novel nanomaterials and development of their surface modification techniques, numerous building blocks will be applied to the graphene-based LbL assembly, and provide a new concept of nanocomposites and novel future applications.

3. CONCLUSION

We have presented a field manual for the LbL assembly of graphene-based multilayer nanocomposites based on the experience and knowledge gained in the course of our previous studies. Graphene-based LbL nanocomposites have been successfully demonstrated with graphene, polymer, and metal NP, and proper strategies for the formation of electrostatic interactions between each component and the graphene layer have been detailed. The LbL assembly of graphene-based nanocomposites is not only limited to the components and

DOI: 10.1021/acs.chemmater.6b02688
Chem. Mater. 2017, 29, 69−79

strategies described in this manual but also can be applied to many of potential counterpart materials, provided their composites with graphene materials are fully rationalized and their preparation is appropriately planned.

The LbL method can be used to optimize device performance by providing a method for adjusting the number of bilayer and internal structures within a functional composite material. Furthermore, it can offer fundamental understanding of the interfaces between graphene and conjugate nanomaterials and provide structural insight into composite engineering at the nanoscale. We anticipate that the detailed protocols outlined in this paper will aid researchers in the design of novel graphene-based nanocomposites with desired and tunable properties.

4. EQUIPMENT SETUP

ζ-Potential. Diluted aqueous suspensions (typical conc. of 0.050 mg mL^{-1}) were prepared in a syringe with 1.0 mL capacity. The solutions were slowly injected into the measurement cell to prevent air bubbles. The syringes were sealed with caps and inserted in the ζ-potential analyzer for colloidal stability measurements.

UV−vis Spectroscopy. UV−vis absorbance was measured with a UV cuvette containing pure DI water as a reference. Diluted aqueous suspensions (0.050 mg mL^{-1}) were prepared in a measurement cuvette, and absorbance was recorded from 200 to 800 nm. As-prepared LbL films assembled on quartz glass were directly measured with a bare quartz slide as a reference. The absorbance range recorded for all samples was from 200 to 800 nm.

SEM. As-prepared LbL assembled films on silicon wafers were coated by Pt sputtering (1 min at 20 mA under vacuum) to increase the electrical conductivity of the samples. SEM images were obtained at an accelerating voltage of 10 kV.

AFM. The target multilayer film was assembled on piranha-cleaned Si wafer to analyze the height and lateral dimensions of the layers with AFM. AFM measurement was performed in the tapping mode at a 1 Hz scan rate.

Ellipsometry. The target film was assembled on a piranha-cleaned Si wafer. The thickness fitting process was performed over a wavelength range of 380 to 900 nm with Cauchy film modeling. As the Cauchy model requires transparency (extinction coefficient < 0.001), measurements were modified with wavelength confinement and B-spline fitting for the qualified results.

Surface Profiler. As-prepared LbL-assembled films on Si wafers were scratched using a cutter to obtain the height of LbL films from the Si substrate. The thickness measurement was performed at a scanning speed of 10 $\mu m\ s^{-1}$ over a frequency range of 5 to 50 Hz.

Cyclic Voltammetry. Electrochemical experiments were performed using a standard three-electrode cell configuration. A platinum wire was used as the counter electrode and an Hg/HgO electrode was used as a reference. The working electrode was a multilayer thin film assembled on ITO-coated glass.

■ ASSOCIATED CONTENT

Supporting Information

The Supporting Information is available free of charge on the ACS Publications website at DOI: 10.1021/acs.chemmater.6b02688.

Experimental preparation for PANi and Au NPs suspensions, characterization of GO sheets, relative charge density calculation of GO(−) in different pH conditions, and list of materials and equipment used in experiment (PDF)

Video clip and snapshots of LbL assembly process (AVI)

■ AUTHOR INFORMATION

Corresponding Author

*B.-S. Kim, e-mail: bskim19@unist.ac.kr.

Author Contributions

The paper was written through contributions of all authors. All authors have given approval to the final version of the paper. All authors contributed equally to this work.

Notes

The authors declare no competing financial interest.

■ ACKNOWLEDGMENTS

This work was supported by the National Research Foundation of Korea (NRF) grant (2014R1A2A1A11052829 and 2015R1A2A2A04003160). E. Ahn, M. Gu, and M. Park acknowledge the financial support from the Global Ph.D. Fellowship funded by the NRF (2013H1A2A1033508, 2013H1A2A1033278, 2014H1A2A1018269).

■ REFERENCES

(1) Geim, A. K.; Novoselov, K. S. The Rise of Graphene. *Nat. Mater.* **2007**, *6*, 183−191.

(2) Nair, R. R.; Blake, P.; Grigorenko, A. N.; Novoselov, K. S.; Booth, T. J.; Stauber, T.; Peres, N. M. R.; Geim, A. K. Fine Structure Constant Defines Visual Transparency of Graphene. *Science* **2008**, *320*, 1308.

(3) Sun, Y.; Wu, Q.; Shi, G. Graphene Based New Energy Materials. *Energy Environ. Sci.* **2011**, *4*, 1113−1132.

(4) Huang, X.; Qi, X.; Boey, F.; Zhang, H. Graphene-Based Composites. *Chem. Soc. Rev.* **2012**, *41*, 666−686.

(5) Chung, C.; Kim, Y.-K.; Shin, D.; Ryoo, S.-R.; Hong, B. H.; Min, D.-H. Biomedical Applications of Graphene and Graphene Oxide. *Acc. Chem. Res.* **2013**, *46*, 2211−2224.

(6) Raccichini, R.; Varzi, A.; Passerini, S.; Scrosati, B. The Role of Graphene for Electrochemical Energy Storage. *Nat. Mater.* **2014**, *14*, 271−279.

(7) Novoselov, K. S.; Geim, A. K.; Morozov, S. V.; Jiang, D.; Zhang, Y.; Dubonos, S. V.; Grigorieva, I. V.; Firsov, A. A. Electric Field Effect in Atomically Thin Carbon Films. *Science* **2004**, *306*, 666−669.

(8) Kim, K. S.; Zhao, Y.; Jang, H.; Lee, S. Y.; Kim, J. M.; Ahn, J.-H.; Kim, P.; Choi, J.-Y.; Hong, B. H.; Kim, K. S. Large-Scale Pattern Growth of Graphene Films for Stretchable Transparent Electrodes. *Nature* **2009**, *457*, 706−710.

(9) Bae, S.; Kim, H.; Lee, Y.; Xu, X.; Park, J.-S.; Zheng, Y.; Balakrishnan, J.; Lei, T.; Ri Kim, H.; Song, Y. Il; Kim, Y.-J.; Kim, K. S.; Özyilmaz, B.; Ahn, J.-H.; Hong, B. H.; Iijima, S. Roll-to-Roll Production of 30-Inch Graphene Films for Transparent Electrodes. *Nat. Nanotechnol.* **2010**, *5*, 574−578.

(10) Hummers, W. S.; Offeman, R. E. Preparation of Graphitic Oxide. *J. Am. Chem. Soc.* **1958**, *80*, 1339−1339.

(11) Lotya, M.; Hernandez, Y.; King, P. J.; Smith, R. J.; Nicolosi, V.; Karlsson, L. S.; Blighe, F. M.; De, S.; Wang, Z.; McGovern, I. T.; Duesberg, G. S.; Coleman, J. N. Liquid Phase Production of Graphene by Exfoliation of Graphite in Surfactant/Water Solutions. *J. Am. Chem. Soc.* **2009**, *131*, 3611−3620.

(12) Loh, K. P.; Bao, Q.; Ang, P. K.; Yang, J. The Chemistry of Graphene. *J. Mater. Chem.* **2010**, *20*, 2277−2289.

(13) Marcano, D. C.; Kosynkin, D. V.; Berlin, J. M.; Sinitskii, A.; Sun, Z.; Slesarev, A.; Alemany, L. B.; Lu, W.; Tour, J. M. Improved Synthesis of Graphene Oxide. *ACS Nano* **2010**, *4*, 4806−4814.

DOI: 10.1021/acs.chemmater.6b02688
Chem. Mater. 2017, 29, 69−79

(14) Dai, L.; Chang, D. W.; Baek, J.-B.; Lu, W. Carbon Nanomaterials for Advanced Energy Conversion and Storage. *Small* **2012**, *8*, 1130−1166.
(15) David, L.; Bhandavat, R.; Singh, G. MoS_2/Graphene Composite Paper for Sodium-Ion Battery Electrodes. *ACS Nano* **2014**, *8*, 1759−1770.
(16) Ji, J.; Zhang, L. L.; Ji, H.; Li, Y.; Zhao, X.; Bai, X.; Fan, X.; Zhang, F.; Ruoff, R. S. Nanoporous $Ni(OH)_2$ Thin Film on 3D Ultrathin-Graphite Foam for Asymmetric Supercapacitor. *ACS Nano* **2013**, *7*, 6237−6243.
(17) Wang, H.; Hu, Y. H. Graphene as a Counter Electrode Material for Dye-Sensitized Solar Cells. *Energy Environ. Sci.* **2012**, *5*, 8182−8188.
(18) Kuila, T.; Bose, S.; Khanra, P.; Mishra, A. K.; Kim, N. H.; Lee, J. H. Recent Advances in Graphene-Based Biosensors. *Biosens. Bioelectron.* **2011**, *26*, 4637−4648.
(19) Shen, J.; Zhu, Y.; Yang, X.; Li, C. Graphene Quantum Dots: Emergent Nanolights for Bioimaging, Sensors, Catalysis and Photovoltaic Devices. *Chem. Commun.* **2012**, *48*, 3686−3699.
(20) Sun, X.; Liu, Z.; Welsher, K.; Robinson, J. T.; Goodwin, A.; Zaric, S.; Dai, H. Nano-Graphene Oxide for Cellular Imaging and Drug Delivery. *Nano Res.* **2008**, *1*, 203−212.
(21) Bao, H.; Pan, Y.; Ping, Y.; Sahoo, N. G.; Wu, T.; Li, L.; Li, J.; Gan, L. H. Chitosan-Functionalized Graphene Oxide as a Nanocarrier for Drug and Gene Delivery. *Small* **2011**, *7*, 1569−1578.
(22) Decher, G. Fuzzy Nanoassemblies: Toward Layered Polymeric Multicomposites. *Science* **1997**, *277*, 1232−1237.
(23) Hammond, P. T. Form and Function in Multilayer Assembly: New Applications at the Nanoscale. *Adv. Mater.* **2004**, *16*, 1271−1293.
(24) Jiang, C.; Markutsya, S.; Tsukruk, V. V. Compliant, Robust, and Truly Nanoscale Free-Standing Multilayer Films Fabricated Using Spin-Assisted Layer-by-Layer Assembly. *Adv. Mater.* **2004**, *16*, 157−161.
(25) Becker, A. L.; Johnston, A. P. R.; Caruso, F. Layer-by-Layer-Assembled Capsules and Films for Therapeutic Delivery. *Small* **2010**, *6*, 1836−1852.
(26) Ariga, K.; Yamauchi, Y.; Rydzek, G.; Ji, Q.; Yonamine, Y.; Wu, K. C.-W.; Hill, J. P. Layer-by-Layer Nanoarchitectonics: Invention, Innovation, and Evolution. *Chem. Lett.* **2014**, *43*, 36−68.
(27) Richardson, J. J.; Bjornmalm, M.; Caruso, F. Technology-Driven Layer-by-Layer Assembly of Nanofilms. *Science* **2015**, *348*, 411.
(28) Xiao, F.-X.; Pagliaro, M.; Xu, Y.-J.; Liu, B. Layer-by-Layer Assembly of Versatile Nanoarchitectures with Diverse Dimensionality: A New Perspective for Rational Construction of Multilayer Assemblies. *Chem. Soc. Rev.* **2016**, *45*, 3088−3121.
(29) Marmisolle, W. A.; Azzaroni, O. Recent Developments in the Layer-by-Layer Assembly of Polyaniline and Carbon Nanomaterials for Energy Storage and Sensing Applications. From Synthetic Aspects to Structural and Functional Characterization. *Nanoscale* **2016**, *8*, 9890−9918.
(30) Lee, S. W.; Kim, B.-S.; Chen, S.; Shao-Horn, Y.; Hammond, P. T. Layer-by-Layer Assembly of All Carbon Nanotube Ultrathin Films for Electrochemical Applications. *J. Am. Chem. Soc.* **2009**, *131*, 671−679.
(31) Kim, B.-S.; Lee, S. W.; Yoon, H.; Strano, M. S.; Shao-Horn, Y.; Hammond, P. T. Pattern Transfer Printing of Multiwalled Carbon Nanotube Multilayers and Application in Biosensors. *Chem. Mater.* **2010**, *22*, 4791−4797.
(32) Sukhishvili, S. A.; Granick, S. Layered, Erasable, Ultrathin Polymer Films. *J. Am. Chem. Soc.* **2000**, *122*, 9550−9551.
(33) Kim, B.-S.; Park, S. W.; Hammond, P. T. Hydrogen-Bonding Layer-by-Layer-Assembled Biodegradable Polymeric Micelles as Drug Delivery Vehicles from Surfaces. *ACS Nano* **2008**, *2*, 386−392.
(34) Sato, M.; Sano, M. Van Der Waals Layer-by-Layer Construction of a Carbon Nanotube 2D Network. *Langmuir* **2005**, *21*, 11490−11494.
(35) Lee, T.; Min, S. H.; Gu, M.; Jung, Y. K.; Lee, W.; Lee, J. U.; Seong, D. G.; Kim, B. Layer-by-Layer Assembly for Graphene-Based Multilayer Nanocomposites: Synthesis and Applications. *Chem. Mater.* **2015**, *27*, 3785−3796.
(36) Kotov, N. A.; Dékány, I.; Fendler, J. H. Ultrathin Graphite Oxide - Polyelectrolyte Composites Prepared by Self - Assembly: Non - Conductive States. *Adv. Mater.* **1996**, *8*, 637−641.
(37) Kovtyukhova, N. I.; Ollivier, P. J.; Martin, B. R.; Mallouk, T. E.; Chizhik, S. a.; Buzaneva, E. V.; Gorchinskiy, A. D. Layer-by-Layer Assembly of Ultrathin Composite Films from Micron-Sized Graphite Oxide Sheets and Polycations. *Chem. Mater.* **1999**, *11*, 771−778.
(38) Kim, J.; Lee, S. W.; Hammond, P. T.; Shao-Horn, Y. Electrostatic Layer-by-Layer Assembled Au Nanoparticle/MWNT Thin Films: Microstructure, Optical Property, and Electrocatalytic Activity for Methanol Oxidation. *Chem. Mater.* **2009**, *21*, 2993−3001.
(39) Hong, J.; Char, K.; Kim, B. S. Hollow Capsules of Reduced Graphene Oxide Nanosheets Assembled on a Sacrificial Colloidal Particle. *J. Phys. Chem. Lett.* **2010**, *1*, 3442−3445.
(40) Kulkarni, D. D.; Choi, I.; Singamaneni, S. S.; Tsukruk, V. V. Graphene Oxide-Polyelectrolyte Nanomembranes. *ACS Nano* **2010**, *4*, 4667−4676.
(41) Ji, Q.; Honma, I.; Paek, S. M.; Akada, M.; Hill, J. P.; Vinu, A.; Ariga, K. Layer-by-Layer Films of Graphene and Ionic Liquids for Highly Selective Gas Sensing. *Angew. Chem., Int. Ed.* **2010**, *49*, 9737−9739.
(42) Lee, D. W.; Hong, T.-K.; Kang, D.; Lee, J.; Heo, M.; Kim, J. Y.; Kim, B.-S.; Shin, H. S. Highly Controllable Transparent and Conducting Thin Films Using Layer-by-Layer Assembly of Oppositely Charged Reduced Graphene Oxides. *J. Mater. Chem.* **2011**, *21*, 3438−3442.
(43) Choi, Y.; Gu, M.; Park, J.; Song, H.-K.; Kim, B.-S. Graphene Multilayer Supported Gold Nanoparticles for Efficient Electrocatalysts Toward Methanol Oxidation. *Adv. Energy Mater.* **2012**, *2*, 1510−1518.
(44) Zhu, J.; Zhang, H.; Kotov, N. A. Thermodynamic and Structural Insights into Nanocomposites Engineering by Comparing Two Materials Assembly Techniques for Graphene. *ACS Nano* **2013**, *7*, 4818−4829.
(45) Jung, Y. K.; Lee, T.; Shin, E.; Kim, B.-S. Highly Tunable Aptasensing Microarrays with Graphene Oxide Multilayers. *Sci. Rep.* **2013**, *3*, 3367.
(46) Park, B.; Lee, W.; Lee, E.; Min, S. H.; Kim, B.-S. Highly Tunable Interfacial Adhesion of Glass Fiber by Hybrid Multilayers of Graphene Oxide and Aramid Nanofiber. *ACS Appl. Mater. Interfaces* **2015**, *7*, 3329−3334.
(47) Jo, K.; Gu, M.; Kim, B.-S. Ultrathin Supercapacitor Electrode Based on Reduced Graphene Oxide Nanosheets Assembled with Photo-Cross-Linkable Polymer: Conversion of Electrochemical Kinetics in Ultrathin Films. *Chem. Mater.* **2015**, *27*, 7982−7989.
(48) Stankovich, S.; Dikin, D. A.; Dommett, G. H. B.; Kohlhaas, K. M.; Zimney, E. J.; Stach, E. A.; Piner, R. D.; Nguyen, S. T.; Ruoff, R. S. Graphene-Based Composite Materials. *Nature* **2006**, *442*, 282−286.
(49) Shao, Y.; Wang, J.; Wu, H.; Liu, J.; Aksay, I. A.; Lin, Y. Graphene Based Electrochemical Sensors and Biosensors: A Review. *Electroanalysis* **2010**, *22*, 1027−1036.
(50) Xu, Y.; Bai, H.; Lu, G.; Li, C.; Shi, G. Flexible Graphene Films via the Filtration of Water-Soluble Noncovalent Functionalized Graphene Sheets. *J. Am. Chem. Soc.* **2008**, *130*, 5856−5857.
(51) Hwang, H.; Joo, P.; Kang, M. S.; Ahn, G.; Han, J. T.; Kim, B.-S.; Cho, J. H. Highly Tunable Charge Transport in Layer-by-Layer Assembled Graphene Transistors. *ACS Nano* **2012**, *6*, 2432−2440.
(52) Park, M.; Lee, T.; Kim, B.-S. Covalent Functionalization Based Heteroatom Doped Graphene Nanosheet as a Metal-Free Electrocatalyst for Oxygen Reduction Reaction. *Nanoscale* **2013**, *5*, 12255−12260.
(53) Stockton, W. B.; Rubner, M. F. Molecular-Level Processing of Conjugated Polymers. 4. Layer-by-Layer Manipulation of Polyaniline via Hydrogen-Bonding Interactions. *Macromolecules* **1997**, *30*, 2717−2725.
(54) Gittins, D. I.; Caruso, F. Spontaneous Phase Transfer of Nanoparticulate Metals from Organic to Aqueous Media. *Angew. Chem., Int. Ed.* **2001**, *40*, 3001−3004.

DOI: 10.1021/acs.chemmater.6b02688
Chem. Mater. 2017, 29, 69−79

(55) Schneider, G.; Decher, G. Functional Core/Shell Nanoparticles via Layer-by-Layer Assembly. Investigation of the Experimental Parameters for Controlling Particle Aggregation and for Enhancing Dispersion Stability. *Langmuir* **2008**, *24*, 1778−1789.
(56) Wang, Y.; Guan, X. N.; Wu, C.-Y.; Chen, M.-T.; Hsieh, H.-H.; Tran, H. D.; Huang, S.-C.; Kaner, R. B. Processable Colloidal Dispersions of Polyaniline-Based Copolymers for Transparent Electrodes. *Polym. Chem.* **2013**, *4*, 4814−4820.
(57) Chen, S.-A.; Hwang, G.-W. Water-Soluble Self-Acid-Doped Conducting Polyaniline - Structure and Properties. *J. Am. Chem. Soc.* **1995**, *117*, 10055−10062.
(58) Dubas, S. T.; Schlenoff, J. B. Swelling and Smoothing of Polyelectrolyte Multilayers by Salt. *Langmuir* **2001**, *17*, 7725−7727.
(59) Shiratori, S. S.; Rubner, M. F. pH-Dependent Thickness Behavior of Sequentially Adsorbed Layers of Weak Polyelectrolytes. *Macromolecules* **2000**, *33*, 4213−4219.
(60) Konkena, B.; Vasudevan, S. Understanding Aqueous Dispersibility of Graphene Oxide and Reduced Graphene Oxide through pKa Measurements. *J. Phys. Chem. Lett.* **2012**, *3*, 867−872.
(61) Podsiadlo, P.; Michel, M.; Lee, J.; Verploegen, E.; Wong Shi Kam, N.; Ball, V.; Lee, J.; Qi, Y.; Hart, A. J.; Hammond, P. T.; Kotov, N. A. Exponential Growth of LBL Films with Incorporated Inorganic Sheets. *Nano Lett.* **2008**, *8*, 1762−1770.
(62) Gu, M.; Lee, J.; Kim, Y.; Kim, J. S.; Jang, B. Y.; Lee, K. T.; Kim, B.-S. Inhibiting the Shuttle Effect in Lithium−sulfur Batteries Using a Layer-by-Layer Assembled Ion-Permselective Separator. *RSC Adv.* **2014**, *4*, 46940−46946.
(63) Lee, T.; Yun, T.; Park, B.; Sharma, B.; Song, H.-K.; Kim, B.-S. Hybrid Multilayer Thin Film Supercapacitor of Graphene Nanosheets with Polyaniline: Importance of Establishing Intimate Electronic Contact through Nanoscale Blending. *J. Mater. Chem.* **2012**, *22*, 21092−21099.

DOI: 10.1021/acs.chemmater.6b02688
Chem. Mater. 2017, 29, 69−79